Dual Stage Image Analysis for a complex pattern classification task: Ham veining defect detection

Jessica F. Lopes [a,*], *Ana Paula A.C. Barbon* [b], *Giorgia Orlandi* [c], *Rosalba Calvini* [c], *Domenico P. Lo Fiego* [c], *Alessandro Ulrici* [c], *Sylvio Barbon Jr.* [a]

[a] *Department of Computer Science, Londrina State University (UEL), Londrina, Brazil*
[b] *Department of Zootechnology, Londrina State University (UEL), Londrina, Brazil*
[c] *Department of Life Sciences and Interdepartmental Centre BIOGEST-SITEIA, University of Modena and Reggio Emilia (UNIMORE), Reggio Emilia, Italy*

Veins in pork thigh carcass are directly related to the quality of dry-cured ham, and consequently to its market value. Some veining defects over the surface of raw ham are easily detected by humans and precisely assessed by a specialist. However, the automatic evaluation of raw ham quality by image analysis poses some challenges to the traditional Computer Vision Systems (CVS), many of them grounded on the complex image pattern related to each defect level. To improve the CVS classification performance without overburdening feature extraction, as well as the common machine learning modelling, we propose Dual Stage Image Analysis (DSIA). DSIA is an additional step in a CVS, that was built in two stages based on the "divide and conquer" strategy. The first stage consists of splitting the region of interest into sub-regions to predict the presence of veining. In the second stage, the algorithm computes the number of veining sub-regions to assess the final defect level classification. A total of 194 raw ham samples were used to evaluate the DSIA performance in the experiments. Support Vector Machine and Random Forest algorithms were compared for inducing the classification model using 92 image features. Random Forest model was the best, capable of predicting defect level with 88.10% accuracy using DSIA. Without DSIA, the CVS with RF achieved an accuracy of 63.10%.

Keywords:
Computer Vision System
Machine learning
Pork quality
Raw ham

1. Introduction

Dry-cured ham production requires control of specific quality properties. One of the most important properties is related to the globosity index, whose optimal value should be in the 1.0–1.2 range, as suggested by the literature (Garavaldi, Rossi, & Lo Fiego, 2008; Russo, Lo Fiego, Nanni Costa, & Tassone, 2003; Čandek-Potokar & Škrlep, 2012). Recent work has addressed dry-cured ham for determining the intramuscular fat (IMF) contained in ham slices (Muñoz, Gou, & Fulladosa, 2019). Moreover, research studies have shown that the

* *Corresponding author.*
E-mail addresses: jessicafernandes@uel.br (J.F. Lopes), apbarbon@gmail.com (A.P.A.C. Barbon), giorgia.orlandi@unimore.it (G. Orlandi), rosalba.calvini@unimore.it (R. Calvini), domenicopietro.lofiego@unimore.it (D.P. Lo Fiego), alessandro.ulrici@unimore.it (A. Ulrici), barbon@uel.br (S. Barbon).
https://doi.org/10.1016/j.biosystemseng.2020.01.008

greater the presence of veins in the pork thigh carcass, the greater the adipose cover and the globosity index, both representing essential quality measurements in dry-cured ham industry (Garavaldi et al., 2008). It must be underlined that visual defects like vein presence and red skin, although not affecting the sensory quality of the product, result in a lowering of its value (Russo et al., 2003; Ulrici, Foca, Ielo, Volpelli, & Fiego, 2012; Čandek-Potokar & Škrlep, 2012).

The analysis of meat quality measurements in the industrial process involves multivariate characteristics such as breed, genotype, feeding, pre-slaughter handling, stunning, slaughter method, chilling and storage conditions. Visual inspection is the most popular technique to assign grades or quality labels to pork meat, and is often performed by specialists (da Costa Barbon et al., 2017). However, human inspection is time-consuming, tedious, laborious and a biased evaluation due to the influence of external factors (Barbin et al., 2016). Furthermore, visual inspection needs to be performed by specialised operators with high experience in quality control (Wu et al., 2012). In addition, the visual perception is a subjective method to evaluate meat processing, which does not provide trustworthy results and standardisation of the raw material (Rosenvold & Andersen, 2003; Sun et al., 2016).

To reduce product variation and remain competitive in a quality-sensitive market, an objective quality measurement for pork-derived products is essential (Lu, Tan, Shatadal, & Gerrard, 2000). However, visual inspection is the most applied technique in the food industry to assign grades or quality labels, even though it is a subjective evaluation by trained persons. An alternative is the laboratory evaluation of parameters that require equipment and complex analytical procedures, which are costly and time-consuming (Chen, Cai, Wan, & Zhao, 2011).

In recent decades, several alternatives to human visual inspection have been proposed, and the Computer Vision System (CVS) based on Charge Coupled Device (CCD) sensors is one of the most broadly used. Several effective non-invasive methods to inspect the quality of food and agricultural products have been developed, including the Fluoroscope image of X-ray transmission (Ogawa, Kondo, & Shibusawa, 2003), Magnetic resonance imaging (Fantazzini, Gombia, Schembri, Simoncini, & Virgili, 2009; Manzocco et al., 2013; McCarthy, 2012) and Computed Tomography (Fulladosa, Santos-Garcés, Picouet, & Gou, 2010). These sophisticated methods deliver competitive results and can even outperform traditional CCD sensors when describing samples. However, issues such as high equipment cost, complex hardware calibration and specialised parametrisation for a given food stimulate the adoption of solutions based on CCD. Schoeman, Williams, du Plessis, and Manley (2016) observed that solutions based on X-ray to sort food, especially agricultural commodities, on the basis of their internal characteristics, demand advanced and particular software implementations. Furthermore, veining is only a visual defect, i.e. it only affects the visual aspect of ham. According to Garavaldi et al. (2008), products with visual defects such as the presence of bleeding, veins, red rind, high or poor marbling, once sliced are completely similar to hams without these defects in terms of texture and of olfactory, taste and aroma profiles. Finally, to replace manual inspection of food, the CVS is user-friendly and cost-effective.

CVS is a solution based on hardware and software for digital image processing which aims at providing automatic classification (da Costa Barbon et al., 2017). The advance of this type of solution in food quality classification allows consistent, efficient and cost-effective results (Gerrard, Gao, & Tan, 1996). Moreover, a CVS delivers a suitable solution for industrial food monitoring, since it provides results with non-contact and non-destructive evaluation, fast time of analysis, low costs, high accuracy and precision (Foca et al., 2013; Muñoz et al., 2019; Pu, Sun, Ma, & Cheng, 2015). In this way, strategies and methodologies based on image analysis and CVS are applied to obtain meat quality parameters (Barbon et al., 2016; Mancini & Hunt, 2005) and to classify meat samples (da Costa Barbon et al., 2017). In particular, da Costa Barbon et al. (2017) described the challenge of creating a generalised CVS capable of handling various types of meat and their classification. The authors described that specific environments, setups and muscle types are tricky parameters to deal with, leading to the development of handcrafted solutions for each scenario. Considering the research field of food engineering, Cusano, Napoletano, and Schettini (2016) emphasised that it is essential to combine different descriptors to achieve higher classification accuracy since different visual characteristics vary with changing environmental conditions. From these descriptors, it is expected to be able to create classification models able to mimic the human brain and, consequently, to face the conflicts associated with the classification based on vision, where handcrafted extraction still plays a very important role (Guido, 2018).

Assessing visual defects, such as vein presence and structure, is an additional difficulty for sample classification by CVS (Sánchez, Albarracin, Grau, Ricolfe, & Barat, 2008). The veining defect in raw ham is usually localised under the skin and it can affect a large area of the carcass. Most skin lesions cause the highest percentage of trimming, as veining defects, resulting in a degrading of the product quality (Costa et al., 2008). Considering the standards of acceptable whole dry-cured ham for the market, low-quality products are those with a high presence of veining defect, which can be identified with different levels of vein quantity. Dealing with image representation of veining defects involves the use of complex features for their description. These complex image patterns demand an effective CVS, including the ability to identify the relevant properties to discriminate each class of veining defects.

To provide a suitable classification of veining defect level, we propose Dual Stage Image Analysis (DSIA) based on the "divide and conquer" strategy. The Region of Interest (ROI), i.e. the part of the image including the raw ham skin, is split into sub-regions in order to extract image features from each one of them, supporting a robust image description even in complex image patterns. The First Stage is carried out by Machine Learning recognition over each sub-region. The Second Stage provides the final decision based on a counting strategy. The method was embedded in a CVS with a set of image features based on colour, intensity, histogram analysis, border and texture, and it was evaluated in comparison to traditional CVS (Lu et al., 2000; Mateo et al., 2006; Du & Sun, 2006a; Ulrici et al.,

2012; Chmiel & Słowiński, 2016; da Costa Barbon et al., 2017). To evaluate the First Stage, we compared two different machine learning algorithms as the classifier: Random Forest (RF) and Support Vector Machine (SVM). These methods were applied to discriminate three different veining levels among 194 raw ham samples.

2. Veining defect issues

The production of dry-cured ham must fulfil some quality control parameters, which are based on requirements of the food processing industry. Raw samples are evaluated to identify some defective characteristics which could impact the quality and acceptability of the final product (Russo, Lo Fiego, Nanni Costa, & Tassone, 2004, pp. 16–19). The quality standard is primarily based on characteristics observed before curing. Indeed, quality parameters such as weight, thickness of the adipose and presence of visual defects are influenced by ante-mortem factors (Čandek-Potokar & Škrlep, 2012). Traditional ham evaluation is based on Parma Quality Institute (PQI) standards (Parma Quality Institute, 2017). Following the PQI statements, in the case of inappropriate physical characteristics, the sample is excluded from the dry-curing process line.

A high quality dry-cured ham satisfies appropriate visual aspect requirements. Skin issues and subcutaneous layer defects, e.g. the presence of visible blood vessels (veining defects), are related to products which cannot be sold as whole dry-cured hams, although they can still be used for the production of trays of dry-cured ham slices (Garavaldi et al., 2008), at a lower price. Due to the high quality requirements, carcass lesions have a substantial economic impact in the production systems (Bottacini et al., 2018). According to Russo et al. (2004, pp. 16–19), the veining defect is related to stunning methods and time-delay to refrigerate the carcass (pre-chilling time), which may occur during the dressing process.

The evaluation of veining defects in raw ham is generally based on the quantity of veining, which is expressed in terms of increasing defect levels. Considering the method exposed by Russo et al. (2004, pp. 16–19), three different levels of veining defect were considered. The labelling process was carried out comparing the ham samples with a reference photographic scale in which level 1 (C_1) corresponds to hams with no defect or imperceptible defects; level 2 (C_2) considers samples with slight veining presence and level 3 (C_3) those with clearly visible defects. Figure 1 shows a representative image for each veining level.

Research has shown an increasing presence of defects in raw hams, among which the veining defect has a higher frequency, sometimes reaching worrying levels (Lo Fiego, Nanni Costa, Tassone, & Russo, 2003). Moreover, trimmed hams are classified, and can eventually be rejected, based on visual comparison with PQI photographic standards.

Besides veining defects, the presence of additional skin lesions and marks (Figs. 1(a)–(d)) pose an additional challenge for the correct identification of blood vessels, and consequently for automatic classification. Indeed, spatial features derived from the images of ham samples may also incorporate information related to skin defects different from veining. In this context, it is necessary to develop effective strategies to improve model performances and reduce false positives.

2.1. *Related work*

The food monitoring process demands rigorous quality control due to the high consumer requirements for this type of product. The quality evaluation is commonly carried out by observing characteristics such as appearance, smell, texture and flavour which are often examined by human specialists (Alden, Omid, Rajabipour, Tajeddin, & Firouz, 2019; da Costa Barbon et al., 2017; Huang, Liu, Ngadi, & Gariepy, 2013; Joo, Kim, Hwang, & Ryu, 2013). Among several techniques to support the analysis of food products, visual inspection is the usual one employed to assess aspect-related characteristics (Felin, Jukola, Raulo, Heinonen, & Fredriksson-Ahomaa, 2016; Gomes & Leta, 2012). This technique allows a straightforward evaluation based on panels for easy assessment by trained human assessors. Furthermore, several defects are related to consumer perception which is quite related to the visual aspect of the food product (Borràs et al., 2015). However, the bias of human visual perception, limitations when evaluating multiple samples and environmental interference may lead to an inaccurate subjective evaluation with high variability.

Concerning industrial environment requirements, techniques based on image analysis have been proposed for improving results in quality control. Under reliable process conditions, these approaches provide accurate solutions which can be applied in industrial production (Singh & Singh, 2016). Several CVS have been proposed to automate the inspection of food products based on their aspect dealing with the limitations of visual evaluation by human operators (Lopes, Ludwig, Barbin, Grossmann, & Barbon, 2019; Caballero et al., 2017a,b; da Costa Barbon et al., 2017; Zapotoczny, Szczypiński, & Daszkiewicz, 2016; Ulrici et al., 2012; Du & Sun, 2006b).

Dealing with meat quality assessment requires many indicators to be estimated, like colour and surface texture, which provide important morphological features. In this frame, computer vision has emerged as a useful technique that gives successful results (Caballero et al., 2016; Jackman, Sun, & Allen, 2011; Ávila et al., 2015, pp. 456–465). Caballero et al. (2016) described the advantages of applying machine learning from MRI for studying salt diffusion in Iberian hams. They suggested the use of linear regression techniques of data mining on computational texture features from Gray Level Co-Occurrence Matrix (GLCM) to predict the salt content in Iberian hams. Similarly, Ávila et al. (2015, pp. 456–465) explored texture features from MRI, but for Iberian loin. They proposed the use of features from 3D texture and were able to obtain high correlations with physico–chemical parameters of the loin. Moreover, a comprehensive discussion about the semantic content of the texture features and loins was made. For Jackman et al. (2011), the best opportunities for improving computer vision solutions lie with hyperspectral imaging, due to the capacity of providing additional information. In the same work, they commented that technologies such as MRI or CT are still prohibitively slow and expensive, encouraging the usage of CVS based on cameras in the industrial environment.

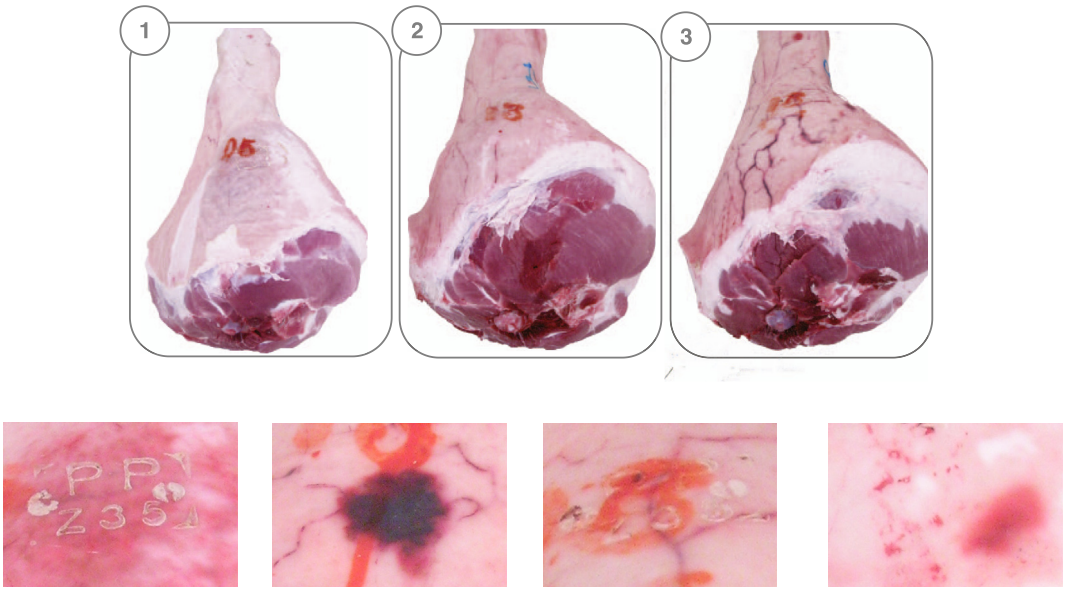

Fig. 1 – Images of raw ham veining defects corresponding to level 1 (C_1), level 2 (C_2) and level 3 (C_3), respectively, and examples of skin lesions: (a) fire marks with traumatic hematoma, (b) non-traumatic hematoma, (c) scratches and (d) meat stamp.

In this context, some CVS approaches have been developed in industrial settings for classifying samples based on quality-related parameters and referring only to the visual aspect, e.g. for the detection of defects (Chmiel & Słowiński, 2016).

Lo Fiego et al. (2007) correlated digital images of pig thighs with some quality attributes of the samples, including mass, length, circumference, thickness of fat and thigh, globosity index and colour of skin. In addition, the presence of veining and red skin defects were also considered in the study to obtain a more comprehensive evaluation of quality attributes. The results obtained did not support automatic thigh classification, demanding more robust techniques. Nonetheless, the authors observed that the higher incidence of the globosity index value is directly related to veining and red skin defects.

Muñoz, Rubio-Celorio, Garcia-Gil, Guàrdia, and Fulladosa (2015) proposed CVS for marbling classification of dry-cured ham. The authors took advantage of machine learning algorithms and image analysis for segmenting intramuscular fat. SVM has shown high classification performance obtaining 89% accuracy. The study did not mention veining defects or their levels.

This study aims at introducing a CVS approach for the classification of raw hams affected by veining defect. The core of the proposed image analysis strategy is based on machine learning techniques applied via a Dual Stage process. Thereby, we propose a technique to improve prediction performance in those problems for which traditional machine learning methods applied to CVS are not sufficient to correctly discriminate the classes of interest.

3. Materials and methods

DSIA is grounded on splitting the original image sample into sub-images, and on the *a posteriori* prediction of a class based on the outcomes resulting from each sub-image. In other words, the subdivision of the original images into sub-images is used to enhance the informational features by converting the complex problem into a less complex one to facilitate the final classification. To present our technique, first we describe the traditional CVS pipeline (Section 3.1). Afterwards, Section 3.2 describes the proposed DSIA approach while Section 3.3 is focused on the evaluation metrics used to support the improvements brought by DSIA.

3.1. *Computer Vision System*

In the experiments, we compared a traditional CVS (Jackman, Sun, & Allen, 2009; O'sullivan et al., 2003; Rodríguez-Pulido, Gordillo, González-Miret, & Heredia, 2013) performance with and without the DSIA technique for classifying raw ham samples in three different veining levels: C_1, C_2 and C_3. CVS can be split into four main steps: Image Acquisition, Image Pre-processing, Feature Extraction and Classification, as showed in Fig. 2. DSIA technique was embedded in the CVS after the pre-processing step to support a better description of complex image patterns. These complex image patterns are composed of different entities, which are challenging to be learnt by a machine learning algorithm, and they may occur at any place and scale in the image.

The proposed DSIA improves the classification performance by extracting patterns from sub-regions of the Region of Interest (ROI) and boosting the original image description with complementary local information. The process is based on the extraction of a feature vector from each image sub-region and on the subsequent application of machine learning decision algorithms on these feature vectors. Thereby, the prediction of the original sample is based on counting the sub-region outcomes, as detailed in Section 3.2.

The image processing steps were performed using ad-hoc routines written in MATLAB environment (The Mathworks

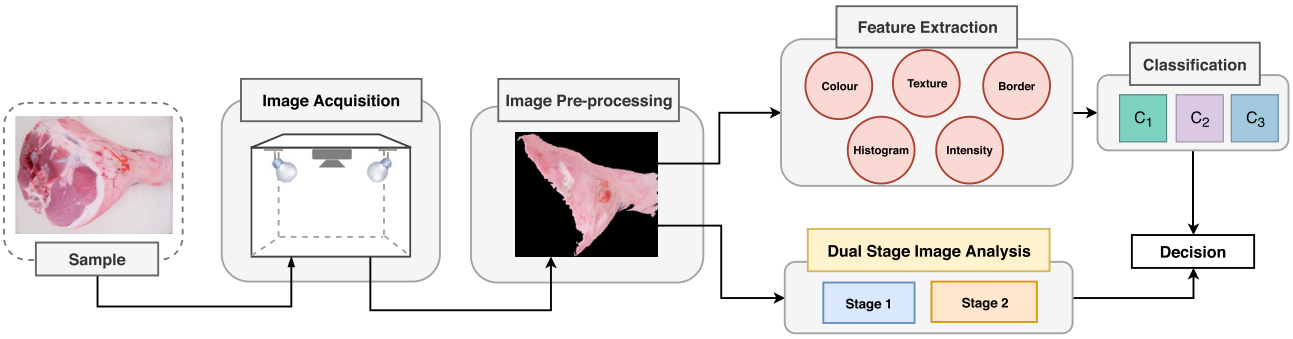

Fig. 2 – Traditional Computer Vision System (gray labels) and Dual Stage Image Analysis technique (orange label) combination for raw ham classification among levels 1, 2 and 3 (C_1, C_2 and C_3). (For interpretation of the references to colour in this figure legend, the reader is referred to the Web version of this article.)

Inc., Natick, MA, USA). Sequentially, the ML classification algorithms were implemented in the R environment. More details are reported in Section 3.1.4. Experiments were conducted with Intel® Core i7-6700 CPU 3.40 GHz 16 GB memory.

3.1.1. *Samples and image acquisition*

A total of 194 raw ham samples, each one derived from a different heavy pig, were collected in a slaughter plant on 5 different days. After carcass slicing, the thighs were stored at 0–4°C for 24 h and subsequently trimmed. Images of the external surface of each thigh were acquired using a Nikon Coolpix 5400 camera with a 5.8–24 mm focal length in a controlled lighting environment. The lighting consisted of LED lamps (Natural daylight, 100 W) with an angle of 45° between the camera lens and lighting source axis. The camera was located vertically over the sample. The images, with a spatial resolution of 2592 × 1944 pixels, were acquired and stored as jpg files for further processing. The camera settings were as follows: manual exposure with a shutter speed of 1/125 s (zoom and flash functions off) and ISO equal to 200. An overview of image acquisition and final prediction workflow is reported in Fig. 2. Then, the ham samples were labelled according to three different veining levels: Level 1 (C_1), which refers to a limited *Veining* presence (17 samples), Level 2 (C_2), which is related to a moderate veins appearance (92 samples), and Level 3 (C_3), which represents the worst case of *Veining* defect on raw hams (85 samples). Each image was labelled by three expert assessors using the reference method based on the comparison with a photographic standard. The methodology applied consists of a subjective analysis based on the evaluation of the raw ham veining defect intensity in the digital image sample.

3.1.2. *Image Pre-processing*

Image pre-processing was conducted considering 6 subsequent steps, with the aim of identifying and segmenting the region of interest in each image, as shown in Fig. 3. Indeed, the isolation of the pigskin from the background and other components of the thigh was not an easy task, due to colour similarities with some parts of ham fat and muscle.

Step 1 of the pre-processing procedure was performed by means of the colourgrams approach (Antonelli et al., 2004) through a Graphical User Interface (Calvini, Orlandi, Foca, & Ulrici, 2019) in order to obtain a general overview of the colour properties of the samples images. Basically, this approach consists of converting each RGB image of the dataset into a 4900-point long signal, namely the colourgram (Foca, Masino, Antonelli, & Ulrici, 2011; Ulrici et al., 2012; Orlandi, Calvini, Foca, & Ulrici, 2018a,b). Each colourgram is obtained by merging in sequence the frequency distribution curves of the R, G and B channels, and of additional colour parameters derived from RGB. These parameters include: the lightness, calculated as the sum of the RGB channels; the three relative colours, i.e. relative red, relative green and relative blue, calculated as the ratio between each channel and lightness; hue (H), saturation (S) and value (V), obtained by converting the RGB coordinates into the HSV colour space; the scores obtained by applying Principal Component Analysis to the raw, mean centred and autoscaled RGB matrix. Thus, a dataset of RGB images is converted into a matrix of signals, which in turn can be further analysed in order to obtain a general overview of the colour properties of the samples at the image-level. Furthermore, since the colourgrams are obtained by merging in sequence the frequency distribution curves of several colour parameters, it is possible to identify colour features of interest and visualise them back at the pixel level in the original image domain. A similar approach has also been successfully proposed for the analysis of hyperspectral images (Calvini, Foca, & Ulrici, 2016; Ferrari, Foca, & Ulrici, 2013). In the specific case under investigation, the acquired RGB images of the raw ham samples were converted into colourgrams and the signals were visually inspected in order to identify the colour parameter leading to the optimal segmentation of the ROI. Thanks to the colourgrams approach, it was therefore possible to simultaneously analyse the frequency distribution curves of several colour parameters calculated for all the images of the dataset. Among all the considered colour parameters, relative red allowed the best results to be obtained for removal of the pixels related to the background and ham fat. In more detail, a threshold value equal to 0.36 of relative red was identified through the inspection of the colourgrams: pixels with relative red values lower than the threshold are ascribed to background and ham fat, while pixels with relative red values higher than the threshold are ascribable to muscle and pigskin.

In Step 2, the segmented image (background removed) was converted into a binary image by setting to one all the pixels with a value higher than 0.8 and setting to zero all the

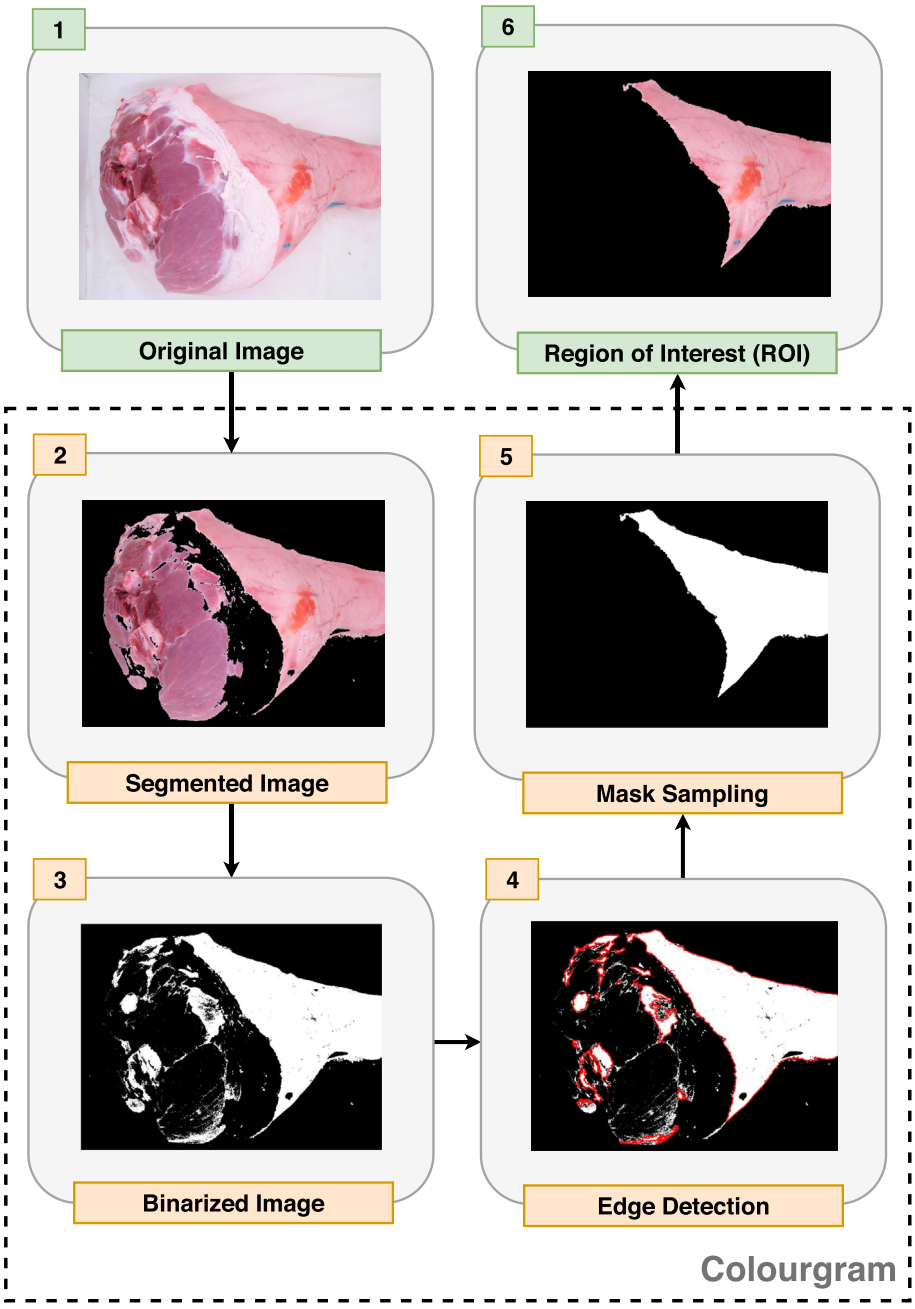

Fig. 3 – Image pre-processing and segmenting for identification of the region of interest (ROI) from raw ham.

remaining pixels. In this way, the areas of the image ascribed to the darker parts of the muscle are eliminated (Step 3). Afterwards, the edges of the objects depicted in the binary image were identified, as shown in Fig. 3 (Step 4). In order to create a mask to identify only the part related to the pigskin of the samples, the boundary of the corresponding object (Step 5) was isolated. As the final step, the mask was applied to the original image, obtaining the region of interest ROI (Step 6).

3.1.3. *Image feature extraction*

After ROI identification, the subsequent step of the image analysis workflow consisted of image feature extraction, as shown in Fig. 2. A set of 92 image features based on colour (Fan et al., 2013), intensity (Laddi, Sharma, Kumar, & Kapur, 2013), border (Canny, 1986; Sobel, 1978) and texture (Haralick, Shanmugam, & Dinstein, 1973) were extracted from each ROI.

In more detail, 33 different features were obtained from Monochromatic (Intensity), RGB (Red, Green and Blue) and HSV (Hue, Saturation and Value) spaces. Furthermore, 21 features were computed based on standard deviation, kurtosis and skewness from the histogram of Intensity (Gray Level), RGB and HSV. The colour channels were analysed separately, and additional features were used to support the prediction. In fact, the colour information of an image is characterised by distribution moments which could be used as image features

for classification (Li, Li, Wang, & Zhu, 2015). Therefore, statistical moments from the colour spaces were included in the considered features. Correlations between channels were also generated to improve the power of properties extracted of each sub-sample.

The entropy value was calculated for the intensity channel, following Kapur, Sahoo, and Wong (1985). Likewise, 19 texture descriptors were calculated according to different approaches to texture analysis: Local Binary Patterns (LBP), Gray Level Co-occurrence Matrix (GLCM) and Fast Fourier Transform (FFT) (Haralick et al., 1973; Nixon & Aguado, 2012; Shen, Chen, & Chang, 2013). LBP is an operator that describes local image texture features. This method turns the specific local texture into a binary vector encoded comparing a gray-scale pixel and the neighbours (Ojala, Pietikäinen, & Mäenpää, 2002). Likewise, GLCM allows mapping patterns over the image. The presence of veining defects imparts peculiar spatial features, which help in distinguishing the veining levels.

Sobel (1978) and Canny (1986) operators supported the extraction of border information (4 features). The number of white pixels present and Hu moments were properties of filtered image by Sobel and Canny to address high contrast regions such as dark veining occurrence and the final defect level. The list including all image features explored is shown in Table 1. The final feature vector for the classification step was obtained by merging all features.

3.1.4. *Classification model*

A classification model provides the final decision for a given sample based on its image feature vector (Barbin et al., 2016). Several research studies have applied machine learning algorithms to create classification models with highly accurate results. Machine Learning is the process of learning from instances and inducting a model toward an automatic classification (Kotsiantis, Zaharakis, & Pintelas, 2007). In our experiment, we compared Support Vector Machine (SVM) and Random Forest (RF) algorithms. These algorithms were chosen due to the particularities of the problem (Barbin et al., 2016; Barbon et al., 2016; Pereira, Barbon, Valous, & Barbin, 2018; Salazar, Toledo, Oñate, & Morán, 2015).

Support Vector Machine (SVM) is a statistical learning algorithm proposed by Vapnik (1995). Belonging to the kernel-based methods, the main principle of SVM consists of finding the best hyperplane which separates the data into respective classes. Random Forest (RF) is an ensemble learning method that was proposed by Breiman (2001). The main idea behind RF consists of combining many decision tree models into a forest for providing more accurate prediction results. In our experiments, we applied algorithms developed in the R environment to induce models for classification. The algorithm descriptions and the corresponding packages used to implement each ML algorithm are briefly described in Table 2.

3.2. *Dual Stage Image Analysis*

Dealing with the classification of complex image patterns requires a powerful description of a given sample toward creating a reliable decision boundary. This is a challenging task, generally addressed by feature extraction considering only the ROI. However, ROI's features may not provide sufficient information to distinguish the different classes, decreasing the predictive performance of classification algorithms. Dual Stage Image Analysis is proposed to improve the image classification task when dealing with complex patterns, like the classification of ham samples according to veining defect levels.

DSIA is based on the assumption that to obtain a better comprehension of the sample image features, the ROI should be split into sub-regions and each sub-region needs to be analysed. Our technique splits the image into several sub-regions to extract local image features from them. The strategy of DSIA follows the "divide and conquer" procedure to transform the main problem into smaller sub-problems to improve the description capacity, even reducing the prediction complexity and bias when analysing the image at once. There are alternatives to our proposal, such as solutions able to boost the feature vector descriptive power, overlooking the specificities of classifiers, e.g. Paraconsistent Feature Engineering (Guido, 2018). However, our strategy is a simple and straightforward method to extract image features, and we obtained both valuable insights from descriptors and competitive results.

Like traditional CVS, DSIA is also a supervised modelling technique. For this reason, a calibration phase is necessary before using it in prediction. This phase requires a supervisor able to label some samples and to identify veining related pixels. In other words, when performing the labelling step for traditional CVS, a human assessor is required to assign each sample to a class. On the other hand, within DSIA, a given label is related to a sub-region considering the presence or absence of a pattern, e.g. veining related pixels. To automate and reduce the cost of labelling each sub-region, we recommend using a ground-truth approach to determine the class assignation, as suggested by Bowyer (2000).

There are two main stages in DSIA, as shown in Fig. 4. The First Stage addresses the segmented sub-regions and their predictions. The Second Stage uses a threshold over the counting of veining sub-regions to provide a final classification.

- *First Stage*: This stage focuses on sub-regions prediction. In calibration, DSIA requires an image with veining marks to automatically label the sub-regions. In other words, a segmented sub-region with veining presence is labelled as Veining. On the other hand, if the sub-region has no veining mark, it is labelled as Non-Veining. The size of sub-regions is a user-defined parameter, which is related to representability of an observed pattern, e.g. a veining image pattern. Very small regions are not able to describe a given pattern and huge regions deliver less precise feature vectors. The labelled sub-regions have their features extracted, and a machine learning model is induced to predict them as Veining or Non-Veining. In the prediction phase, the induced model is used throughout all sub-regions from a single ROI to provide the number of Veining regions for further classification. When dealing with sub-regions prediction, the problem of multi-class classification is transformed into a binary classification problem in the First Stage. Though the original classification remains at the focus of the DSIA,

Table 1 – List of all image features explored for raw ham classification.

No.	Type	Name	Description
1	Colour	cor RG	Correlation between Red and Green channel
2	Colour	cor RB	Correlation between Red and Blue channel
3	Colour	cor RH	Correlation between Red and Hue channel
4	Colour	cor RS	Correlation between Red and Saturation channel
5	Colour	cor RV	Correlation between Red and Value channel
6	Colour	cor RI	Correlation between Red and Intensity channel
7	Colour	cor GB	Correlation between Green and Blue channel
8	Colour	cor GH	Correlation between Green and Hue channel
9	Colour	cor GS	Correlation between Green and Saturation channel
10	Colour	cor GV	Correlation between Green and Value channel
11	Colour	cor GI	Correlation between Green and Intensity channel
12	Colour	cor BH	Correlation between Blue and Hue channel
13	Colour	cor BS	Correlation between Blue and Saturation channel
14	Colour	cor BV	Correlation between Blue and Value channel
15	Colour	cor BI	Correlation between Blue and Intensity channel
16	Colour	cor HS	Correlation between Hue and Saturation channel
17	Colour	cor HV	Correlation between Hue and Value channel
18	Colour	cor HI	Correlation between Hue and Intensity channel
19	Colour	cor SV	Correlation between Saturation and Value channel
20	Colour	cor SI	Correlation between Saturation and Intensity channel
21	Colour	cor VI	Correlation between Value and Intensity channel
22	Colour	mean H	Mean of Hue channel
23	Colour	std H	Standard Deviation of Hue channel
24	Colour	mean S	Mean of Saturation channel
25	Colour	std S	Standard Deviation of Saturation channel
26	Colour	mean V	Mean of Value channel
27	Colour	std V	Standard Deviation of Value channel
28	Colour	mean R	Mean of Red channel
29	Colour	std R	Standard Deviation of Red channel
30	Colour	mean G	Mean of Green channel
31	Colour	std G	Standard Deviation of Green channel
32	Colour	mean B	Mean of Blue channel
33	Colour	std B	Standard Deviation of Blue channel
34	Intensity	mean I	Mean of Intensity channel
35	Intensity	std I	Standard Deviation of Intensity channel
36	Intensity	entropy I	Entropy of Intensity channel
37	Histogram	std hist H	Standard Deviation of Histogram of Hue channel
38	Histogram	kurt hist H	Kurtosis of Histogram of Hue channel
39	Histogram	skew hist H	Skewness of Histogram of Hue channel
40	Histogram	std hist S	Standard Deviation of Histogram of Saturation channel
41	Histogram	kurt hist S	Kurtosis of Histogram of Saturation channel
42	Histogram	skew hist S	Skewness of Histogram of Saturation channel
43	Histogram	std hist V	Standard Deviation of Histogram of Value channel
44	Histogram	kurt hist V	Kurtosis of Histogram of Value channel
45	Histogram	skew hist V	Skewness of Histogram of Value channel
46	Histogram	std hist R	Standard Deviation of Histogram of Red channel
47	Histogram	kurt hist R	Kurtosis of Histogram of Red channel
48	Histogram	skew hist R	Skewness of Histogram of Red channel
49	Histogram	std hist G	Standard Deviation of Histogram of Green channel
50	Histogram	kurt hist G	Kurtosis of Histogram of Green channel
51	Histogram	skew hist G	Skewness of Histogram of Green channel
52	Histogram	std hist B	Standard Deviation of Histogram of Blue channel
53	Histogram	kurt hist B	Kurtosis of Histogram of Blue channel
54	Histogram	skew hist B	Skewness of Histogram of Blue channel
55	Histogram	std hist I	Standard Deviation of Histogram of Intensity channel
56	Histogram	kurt hist I	Kurtosis of Histogram of Intensity channel
57	Histogram	skew hist I	Skewness of Histogram of Intensity channel
58	Border	nump sobel	Number of white pixels in Sobel image
59–65	Border	hu sobel1–hu sobel7	Hu Moments of Sobel image
66	Border	nump canny	Number of white pixels in Canny image
67–73	Border	hu canny1–hu canny7	Hu Moments of Canny image
74–83	Texture	lbp 0–lbp 9	LBP Vector
84	Texture	com entropy	Entropy of Co-occurrence Matrix
85	Texture	com inertia	Inertia of Co-occurrence Matrix

Table 1 – (continued)

No.	Type	Name	Description
86	Texture	com energy	Energy of Co-occurrence Matrix
87	Texture	com correlation	Correlation of Co-occurrence Matrix
88	Texture	com homogeneity	Homogeneity of Co-occurrence Matrix
89	Texture	FFT energy	Energy of FFT
90	Texture	FFT entropy	Entropy of FFT
91	Texture	FFT inertia	Inertia of FFT
92	Texture	FFT homogeneity	Homogeneity of FFT

now the decision is based on the number of regions that present or not a picked pattern.

- *Second Stage*: The class identification provided by the supervisor is used in the procedure called Threshold Computation, which takes into account the number of veining regions to detect thresholds allowing the possibility of solving a multi-class problem. This procedure is applied to identify two threshold values, λ_1 and λ_2. The thresholds are computed from the intervals of Probability Density Function (PDF) considering each defect level of raw hams (C_1, C_2 and C_3). Under the assumption that the three classes are equally probable and that the distributions are accurately estimated, λ_1 and λ_2 are the thresholds over the areas of overlap between C_1 and C_2, and between C_2 and C_3, respectively. These thresholds are used as classification boundaries related to the number of Veining sub-regions during the prediction phase. In the case of more levels of defects, the same procedure could be applied by computing more thresholds for each pair of contiguous classes.

DSIA stages are related to "divide and conquer" strategy, transforming the problem to mitigate some pattern recognition issues. Image pre-processing, such as contrast enhancement and denoising, can improve image classification independent of DSIA.

Concerning ROI splitting in the First Stage, in our experiments different sizes of the subregions were evaluated to find the optimal splitting scheme: 10 × 10, 25 × 25, 50 × 50, 75 × 75 and 100 × 100 pixels. The image features extracted from each sub-region are reported in Section 3.1.3. It is important to mention that the samples were randomly split into a training set, including 110 samples (57% of total samples), for the calibration phase and a test set containing 84 samples (43% of total samples) to evaluate the results in prediction. Both RF and SVM were compared in sub-region prediction modelling, as well as in the traditional CVS framework.

3.3. *Evaluation metrics*

The performance of CVS was evaluated using the Total Accuracy method (Accuracy Matrix) (Aggarwal, 2014) which is defined by Equation (1). This metric is computed through the Confusion Matrix, which summarises the outcomes of a classification model.

$$Total\ Accuracy = \frac{TP + TN}{n} \tag{1}$$

Considering the Confusion Matrix, Total Accuracy is obtained from the sum of the elements in the main diagonal. These diagonal values are the True Positive (TP) and True Negative (TN) ones which, observing Equation (1), are divided by the sum of the whole samples (n) of the matrix. Therefore, Total Accuracy allows the performance of the method used to predict the image samples to be estimated. Additionally, Precision (Eq. (2)) and Recall (Eq. (3)) were used to provide a more realistic comparison since the dataset is unbalanced. Those metrics are based on False Positive (FP) and False Negative (FN).

$$Precision = \frac{TP}{TP + FP} \tag{2}$$

$$Recall = \frac{TP}{TP + FN} \tag{3}$$

Finally, it was possible to relate the achieved results with the relevance of the considered image features and machine learning algorithms in raw ham classification. RF importance was considered in this phase, since it estimates the importance of the extracted features through their prediction error, when constructing the ensemble of decision trees inside the Random Forest.

4. Results and discussion

The results of DSIA are presented in comparison with the standard image classification (Traditional CVS) to show the advantages of the proposed method. Subsequently, the results are discussed in terms of the pixel size of the sub-regions, and of the importance of the image features on raw ham veining defect identification. Table 3 summarises the RF and SVM results obtained for the different sub-regions resolutions tested.

CVS coupled with DSIA presented a high performance in the majority of the tested models, except for those calculated with a sub-image resolution of 10 × 10 pixels. The best results were obtained with RF algorithm considering sub-images of 50 × 50 pixels, leading to 88.10% of accuracy, a precision value equal to 92.71% and 85.83% of recall. The worst resolution was 10 × 10 pixels, achieving an accuracy value of 55.95% with RF and 61.91% with SVM, and consequently low values of precision and recall. These results show that considering too small sub-sampling areas causes a loss of important characteristics, which are fundamental to describe the problem at hand. Conversely, larger sub-sampling areas account for more complex spatial patterns, which give the possibility of accounting also for other textural features and/or defects

Table 2 – Machine learning algorithms used in the experiments and corresponding R. packages.

Algorithm	Description	R package	Hyperparameters
Random Forest (RF)	Combination of decision tree models that provides more accurate prediction (Breiman, 2001; Scornet, Biau, & Vert, 2015).	Random Forest	ntree = 100; mtry = 7
Support Vector Machine (SVM)	A statistical learning algorithm (Vapnik, 1995), have achieved important results in food quality solutions (Wang, 2005).	e1071	kernel = polynomial; $\gamma = 0.02$; degree = 3

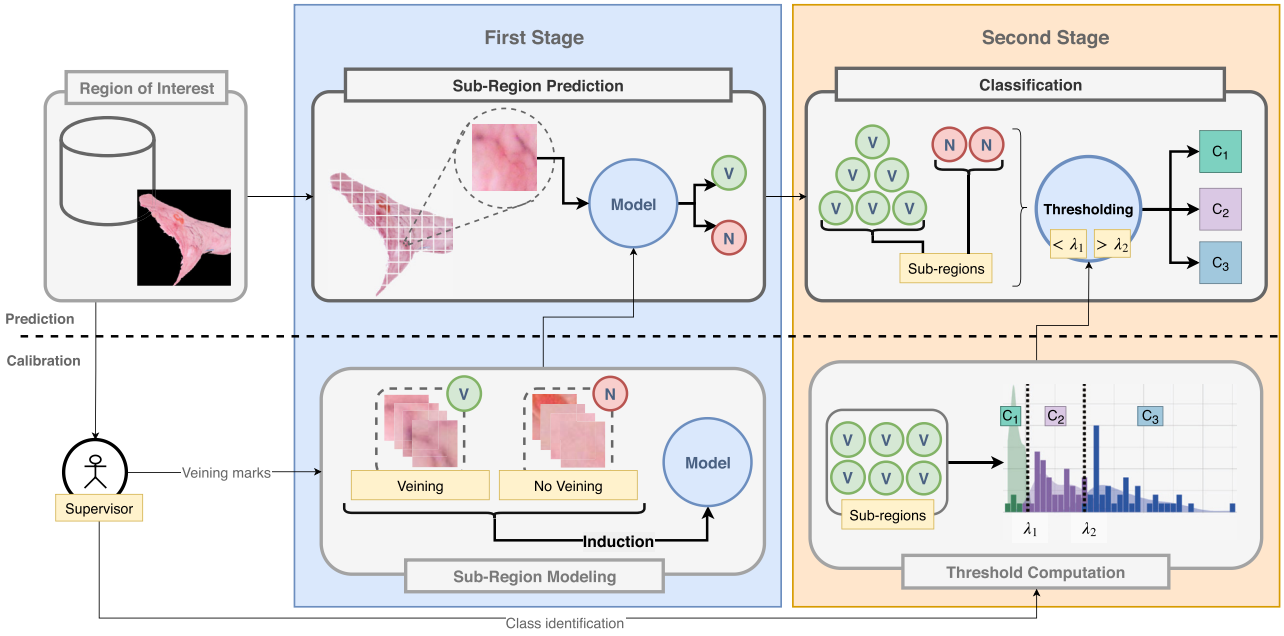

Fig. 4 – Dual Stage overview.

different from veining, causing a decrease in the predictive ability of the method. Considering the traditional CVS approach, RF achieved superior results with 63.10% of accuracy, 44.44% of precision and recall value of 44.55%, slightly better than SVM (61.91%, 43.20% and 43.76%, respectively). Regarding processing time of the methods, traditional CVS required less time to analyse each sample (average of 12.2 s) when compared to the average time of DSIA (33.2 s). DSIA required on the average 2.7 times the computation time of traditional CVS, but its improvement of predictive performance encourage its usage in the industry. Although the time-cost was not the focus of our proposal, a lower-cost feature extraction could be implemented to reduce the time cost. It is important to note that the time comparison was performed based on all image features: dealing with the trade-off between important and low-cost features can reduce the processing time. More details about the importance of the considered features are given in Section 4.1.

The values of λ_1 and λ_2 play an important role in the final classification. In Table 3 both values are shown for the different resolutions and models, while Fig. 5 reports the corresponding probability density functions (PDFs). This figure shows that the best predictive performance obtained considering the resolution of 50 × 50 pixels is related to the lower overlap between the PDFs of the three levels. In the same way, RF 25 × 25, SVM 25 × 25 and RF 50 × 50 presented

Table 3 – Comparison of metrics and thresholds found with different methods and algorithms (RF and SVM) over Prediction dataset.

Method	Sub-region Resolution	RF					SVM				
		Accuracy	Precision	Recall	λ_1	λ_2	Accuracy	Precision	Recall	λ_1	λ_2
Traditional	–	63.10%	44.44%	44.55%	–	–	61.91%	43.20%	43.76%	–	–
DSIA	10 × 10	55.95%	53.44%	68.95%	0.1802	0.2309	61.91%	56.68%	73.18%	0.1858	0.2384
	25 × 25	83.33%	72.91%	82.45%	0.0465	0.0884	82.14%	71.89%	81.60%	0.0454	0.0810
	50 × 50	88.10%	92.71%	85.83%	0.0976	0.1827	83.33%	82.63%	88.33%	0.1034	0.1731
	75 × 75	79.76%	73.02%	74.16%	0.1491	0.2643	78.57%	72.77%	79.14%	0.1475	0.1301
	100 × 100	75.00%	66.87%	70.77%	0.1410	0.2475	84.52%	79.00%	71.60%	0.1163	0.2668

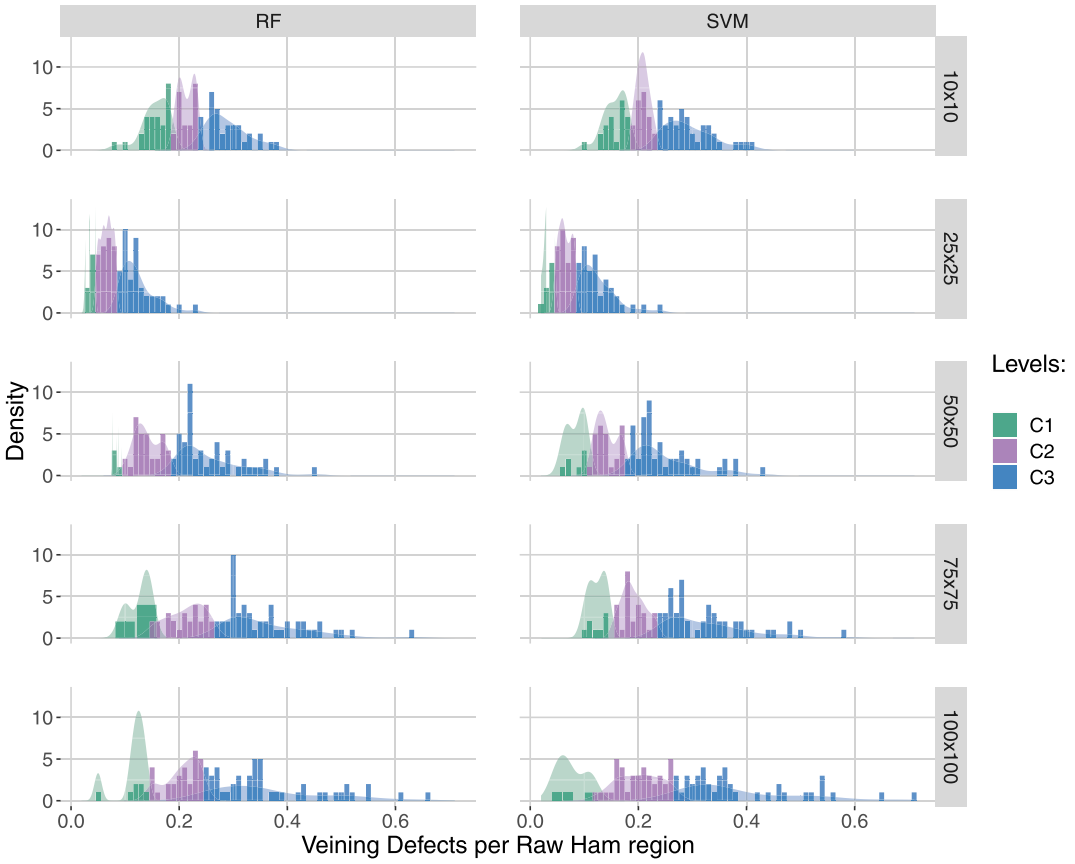

Fig. 5 – Counts and probability density functions for the three veining levels.

Table 4 – Precision and Recall of RF and SVM classification levels per method.

Method	Sub-region Resolution		RF		SVM	
			Precision	Recall	Precision	Recall
Traditional	–	C_1	00.00%	00.00%	00.00%	00.00%
		C_2	58.33%	87.50%	58.18%	80.00%
		C_3	75.00%	46.15%	71.43%	51.28%
DSIA	10 × 10	C_1	18.52%	100.00%	23.81%	100.00%
		C_2	56.52%	32.50%	68.18%	37.50%
		C_3	85.29%	74.36%	78.05%	82.05%
	25 × 25	C_1	40.00%	80.00%	40.00%	80.00%
		C_2	90.63%	72.50%	87.88%	72.50%
		C_3	88.10%	94.87%	87.80%	92.31%
	50 × 50	C_1	100.00%	80.00%	71.43%	100.00%
		C_2	96.88%	77.50%	100.00%	65.00%
		C_3	81.25%	100.00%	76.47%	100.00%
	75 × 75	C_1	50.00%	60.00%	50.00%	80.00%
		C_2	92.59%	62.50%	92.31%	60.00%
		C_3	76.47%	100.00%	76.00%	97.44%
	100 × 100	C_1	42.86%	60.00%	66.67%	40.00%
		C_2	82.76%	60.00%	84.62%	82.50%
		C_3	75.00%	92.31%	85.71%	92.31%

the smallest standard deviation in the number of veining sub-regions per level to compose their PDF. To observe the complexity of each veining level, Table 4 reports the precision and recall values for each sub-region and considering C_1, C_2 and C_3 separately from each other.

The intermediate levels in classification tasks with gradual class dispersion leads to lower performance in comparison to boundary levels. Traditional CVS obtained a biased recall result for veining level C_2, as visible in Table 4 when observing precision and recall metrics and the classification of C_1 level.

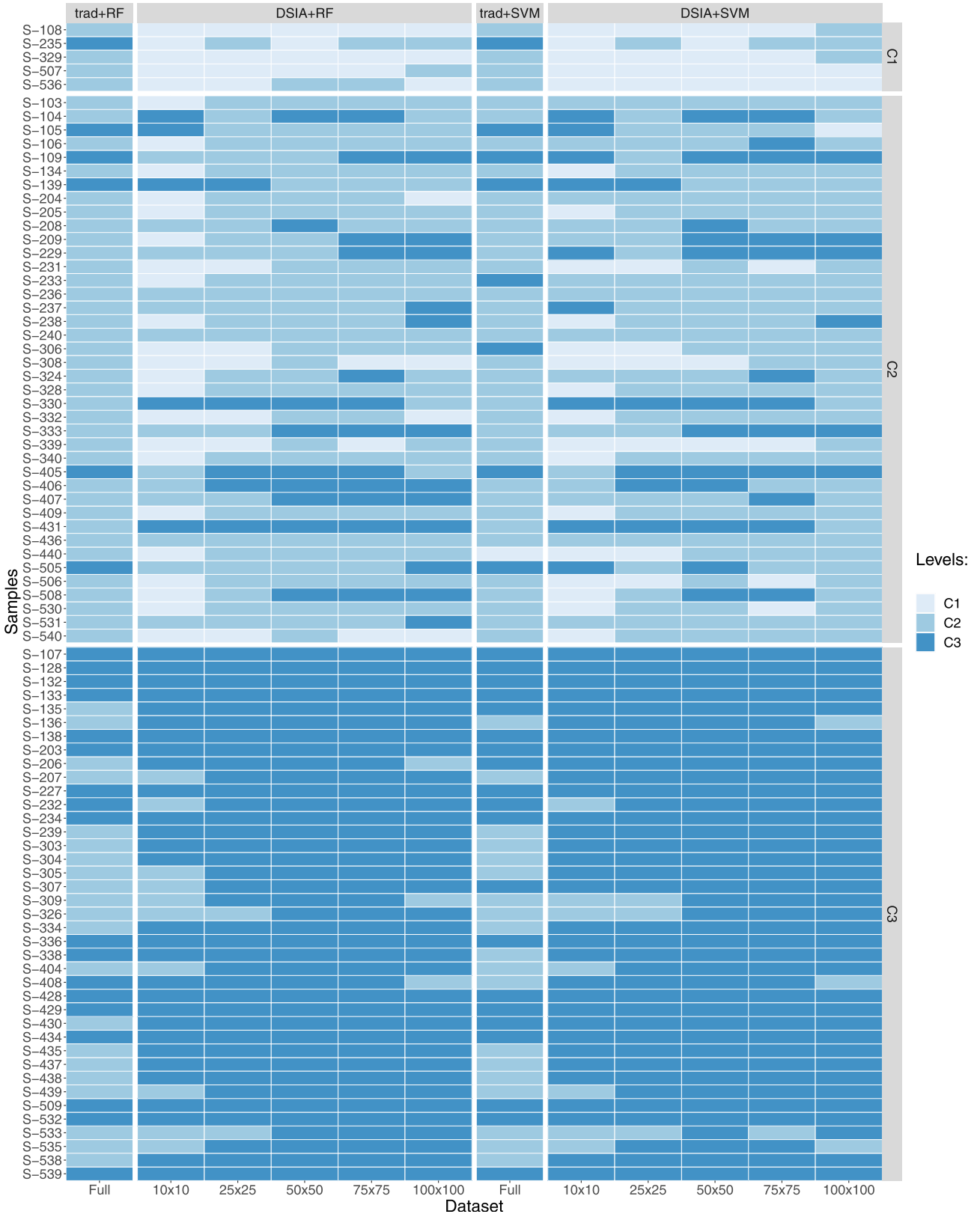

Fig. 6 – Heatmap of prediction set for levels C_1, C_2 and C_3 of RF and SVM comparing DSIA.

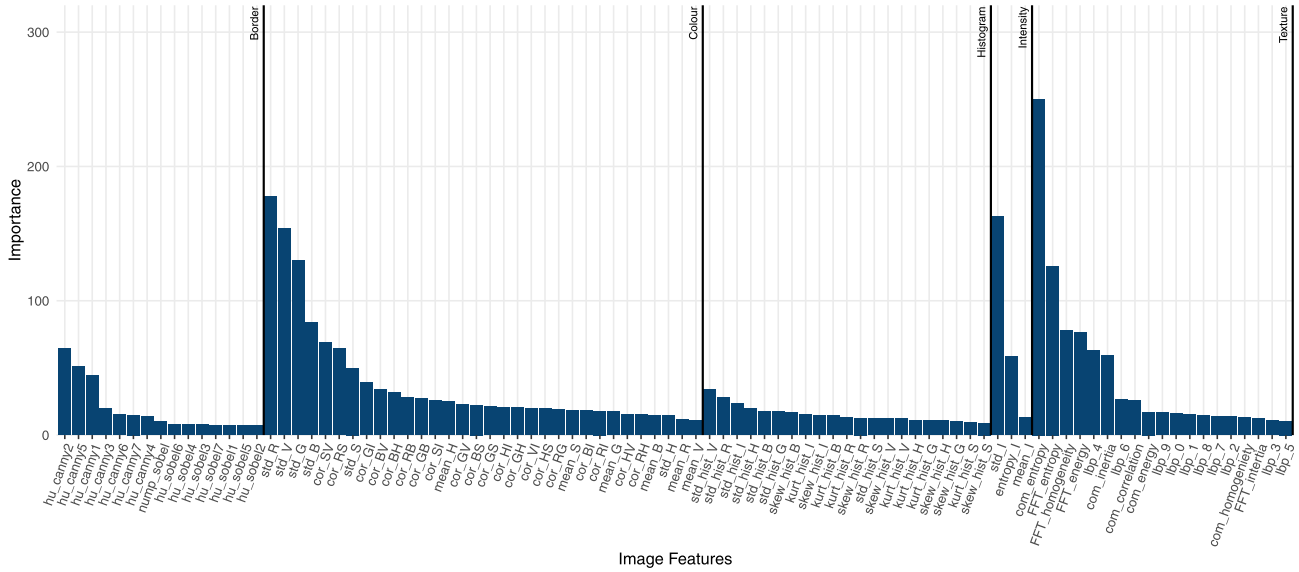

Fig. 7 – Features importance per descriptors.

DSIA with both RF and SVM obtained comparable results, with C_3 being the most easily predictable level, followed by C_1 and by the intermediate class (C_2).

To identify outliers or badly labelled samples, we created a heatmap (Fig. 6) which shows the classification results obtained from all of the raw ham samples. The different shades of blue represent the different veining levels: a lighter blue colour indicates samples predicted as belonging to level C_1, a darker blue colour indicates samples predicted as belonging to level C_3, while the intermediate blue colour is associated with samples predicted as level C_2. An overview of Fig. 6 allows the observation that level C_2 presents the most complex pattern, since it resulted in the most misclassified class.

Considering the results of traditional CVS, slightly better performance was observed with RF in comparison to SVM. The traditional method was not useful in distinguishing among the three classes. The inaccurate classification performance was mainly influenced by the fact that the CVS was not able to correctly classify the samples belonging to level C_1, since they were all assigned to class C_2. The image analysis from the whole ROI smooths the characteristics of vein presence, degrading the image features that allow the properties of the veining level to be specified. Therefore, the use of sub-regions as proposed in DSIA was able to extract the image features to create a better classification approach. Sub-regions with low resolution (10 × 10 pixels) obtained the worst classification results, mainly for class C_2.

Regarding some insights into image features, sub-regions with low resolution are not able to provide a suitable pattern towards its extraction. For example, the most important features are related to entropy of the co-occurrence matrix. When extracting these features from low-resolution sub-regions there is in fact a decrease in texture structure, and consequently the descriptive performance is compromised. A more precise discussion about the relevance of features is made in Section 3.1.3.

4.1. *Feature importance analysis*

As mentioned in Section 3.3, the RF Importance supports the analysis of the most relevant features used for creating the prediction model. Figure 7 reports the RF Importance of the features to classify raw ham defects. The descriptors (Table 1) are sorted by their importance, separately by type: Border, Colour, Histogram, Intensity and Texture, from high to low values.

The features with higher importance were Texture-related ones, in particular the entropy of the co-occurrence matrix. Also some texture features of LBP metrics were efficient for predicting sample levels. Sequentially, the other important features were the Colour-related and Intensity ones, with many scores greater than 50. On average, Colour features are almost equally important as Texture ones. In general, useful information is brought by the synergy between different types of features, which helps to classify the samples according with the different raw ham veining defect levels.

4.2. *DSIA challenges*

The results obtained showed that there was a significant improvement in the predictive performance when using DSIA embedded into a CVS. In particular, the best results were achieved using 50 × 50 pixels of resolution per sub-region. As the size of the sub-region was increased, a decline in performance was observed. While low resolution impairs the sub-regions identification between *veining* and *no veining* defects, high size images decrease the concentration of *veining* defects per region; therefore, the classification performance decreases in both cases. Thus, DSIA is highly dependent on a suitable sub-region resolution for obtaining promising results.

According to the reported results, DSIA demonstrated a superior capability of prediction, compared to using CVS without the DSIA approach. For complex image problems in

which the CVS method is not feasible, image division into smaller regions increases the detail of information about the object of interest. By dividing the images of raw hams into sub-regions, those which display *veining* defects are identified with the usage of a thresholding method to find a suitable number of regions that represent a defect level. On the other hand, the First Stage of DSIA demands images with veining patterns identified to automatically label the sub-regions. This is an additional requirement and disadvantage of DSIA since in the traditional CVS the ROI classification requires just image features and labels concerning the whole sample.

5. Conclusion

DSIA gave a significant improvement over traditional CVS for the identification of veining defects, since it was able to significantly improve the classification performance. Results with RF and sub-regions of 50 pixels outperform the other DSIA configurations, achieving 88.10% accuracy. In comparison to traditional CVS, the improvements obtained by the proposed approach are very clear, since RF without DSIA achieved an accuracy of 63.10%.

The proposed alternative is suitable for production lines in the ham industry and does not require a sophisticated environment for image acquisition based on RGB imaging. A variety of research studies dealing with similar tasks have not been able to achieve the proper image classification of ROIs with the presence of uncontrolled defects such as fire marks, traumatic haematomas, non-traumatic haematomas, scratches or meat stamps. Recognising complex image patterns is a challenge not restricted to food evaluation, but requires diverse research fields toward improving the comprehension and performance of automated solutions supported by computer vision. The "divide and conquer" strategy adopted by DSIA opens new opportunities in the analysis of images composed by complex textures. Future research work aims at comparing the current approach with more recent Deep Learning Image Systems.

Declaration of Competing Interest

The authors declare that they have no known competing financial interests or personal relationships that could have appeared to influence the work reported in this paper.

Acknowledgement

This study was financed in part by the Coordenação de Aperfeiçoamento de Pessoal de Nível Superior - Brasil (CAPES) - Finance Code 001, Coordination for the National Council for Scientific and Technological Development (CNPq) of Brazil - Grant of Project 420562/2018-4 and Fundação Araucária (Paraná, Brazil).

REFERENCES

Aggarwal, C. C. (Ed.). (2014). *Data classification: Algorithms and applications*. CRC Press.

Alden, K. M., Omid, M., Rajabipour, A., Tajeddin, B., & Firouz, M. S. (2019). Quality and shelf-life prediction of cauliflower under modified atmosphere packaging by using artificial neural networks and image processing. *Computers and Electronics in Agriculture, 163*, 104861.

Antonelli, A., Cocchi, M., Fava, P., Foca, G., Franchini, G. C., Manzini, D., et al. (2004). Automated evaluation of food colour by means of multivariate image analysis coupled to a wavelet-based classification algorithm. *Analytica Chimica Acta, 515*(1), 3–13.

Ávila, M. M., Caballero, D., Durán, M. L., Caro, A., Pérez-Palacios, T., & Antequera, T. (2015, July). Including 3D-textures in a computer vision system to analyze quality traits of loin. In *International conference on computer vision systems*. Cham: Springer.

Barbin, D. F., Mastelini, S. M., Barbon, S., Jr., Campos, G. F., Barbon, A. P. A., & Shimokomaki, M. (2016). Digital image analyses as an alternative tool for chicken quality assessment. *Biosystems Engineering, 144*, 85–93.

Barbon, A. P. A., Barbon, S., Jr., Mantovani, R. G., Fuzyi, E. M., Peres, L. M., & Bridi, A. M. (2016). Storage time prediction of pork by computational intelligence. *Computers and Electronics in Agriculture, 127*, 368–375.

Borràs, E., Ferré, J., Boqué, R., Mestres, M., Aceña, L., & Busto, O. (2015). Data fusion methodologies for food and beverage authentication and quality assessment–a review. *Analytica Chimica Acta, 891*, 1–14.

Bottacini, M., Scollo, A., Edwards, S. A., Contiero, B., Veloci, M., Pace, V., et al. (2018). Skin lesion monitoring at slaughter on heavy pigs (170 kg): Welfare indicators and ham defects. *PloS One, 13*(11), e0207115.

Bowyer, K. W. (2000). Validation of medical image analysis techniques. *Handbook of medical imaging, 2*, 567–607.

Breiman, L. (2001). Random forests. *Machine Learning, 45*(1), 5–32.

Caballero, D., Antequera, T., Caro, A., Ávila, M. D. M., G Rodríguez, P., & Perez-Palacios, T. (2017a). Nondestructive analysis of sensory traits of dry-cured loins by MRI–computer vision techniques and data mining. *Journal of the Science of Food and Agriculture, 97*(9), 2942–2952.

Caballero, D., Caro, A., Rodríguez, P. G., Durán, M. L., del Mar Ávila, M., Palacios, R., et al. (2016). Modeling salt diffusion in iberian ham by applying MRI and data mining. *Journal of Food Engineering, 189*, 115–122.

Caballero, D., Pérez-Palacios, T., Caro, A., Amigo, J. M., Dahl, A. B., ErsbØll, B. K., et al. (2017b). Prediction of pork quality parameters by applying fractals and data mining on MRI. *Food Research International, 99*, 739–747.

Calvini, R., Foca, G., & Ulrici, A. (2016). Data dimensionality reduction and data fusion for fast characterization of green coffee samples using hyperspectral sensors. *Analytical and Bioanalytical Chemistry, 408*(26), 7351–7366.

Calvini, R., Orlandi, G., Foca, G., & Ulrici, A. (2019). Colourgrams GUI: A graphical user-friendly interface for the analysis of large datasets of RGB images. *Chemometrics and Intelligent Laboratory Systems*, 103915.

Čandek-Potokar, M., & Škrlep, M. (2012). Factors in pig production that impact the quality of dry-cured ham: A review. *Animal, 6*(2), 327–338.

Canny, J. (1986). A computational approach to edge detection. *IEEE Transactions on Pattern Analysis and Machine Intelligence*, (6), 679–698.

Chen, Q., Cai, J., Wan, X., & Zhao, J. (2011). Application of linear/non-linear classification algorithms in discrimination of pork storage time using fourier transform near infrared (FT-NIR)

spectroscopy. *LWT-Food Science and Technology, 44*(10), 2053–2058.
Chmiel, M., & Słowiński, M. (2016). The use of computer vision system to detect pork defects. *LWT-Food Science and Technology, 73*, 473–480.
Costa, L. N., Tassone, F., Comellini, M., Ielo, M., Fiego, D. L., & Russo, V. (2008). Effect of the slaughterhouse on the incidence of defects in raw pig ham destined to the dry-curing process. *Veterinary Research Communications, 32*(1), 351–353.
Cusano, C., Napoletano, P., & Schettini, R. (2016). Combining multiple features for color texture classification. *Journal of Electronic Imaging, 25*(6), 061410.
da Costa Barbon, A. P. A., Barbon, S., Jr., Campos, G. F. C., Seixas, J. L., Jr., Peres, L. M., Mastelini, S. M., et al. (2017). Development of a flexible computer vision system for marbling classification. *Computers and Electronics in Agriculture, 142*, 536–544.
Du, C. J., & Sun, D. W. (2006a). Automatic measurement of pores and porosity in pork ham and their correlations with processing time, water content and texture. *Meat Science, 72*(2), 294–302.
Du, C. J., & Sun, D. W. (2006b). Learning techniques used in computer vision for food quality evaluation: A review. *Journal of Food Engineering, 72*(1), 39–55.
Fan, F. H., Ma, Q., Ge, J., Peng, Q. Y., Riley, W. W., & Tang, S. Z. (2013). Prediction of texture characteristics from extrusion food surface images using a computer vision system and artificial neural networks. *Journal of Food Engineering, 118*(4), 426–433.
Fantazzini, P., Gombia, M., Schembri, P., Simoncini, N., & Virgili, R. (2009). Use of magnetic resonance imaging for monitoring parma dry-cured ham processing. *Meat Science, 82*(2), 219–227.
Felin, E., Jukola, E., Raulo, S., Heinonen, J., & Fredriksson-Ahomaa, M. (2016). Current food chain information provides insufficient information for modern meat inspection of pigs. *Preventive Veterinary Medicine, 127*, 113–120.
Ferrari, C., Foca, G., & Ulrici, A. (2013). Handling large datasets of hyperspectral images: Reducing data size without loss of useful information. *Analytica Chimica Acta, 802*, 29–39.
Foca, G., Masino, F., Antonelli, A., & Ulrici, A. (2011). Prediction of compositional and sensory characteristics using RGB digital images and multivariate calibration techniques. *Analytica Chimica Acta, 706*(2), 238–245.
Foca, G., Salvo, D., Cino, A., Ferrari, C., Fiego, D. P. L., Minelli, G., et al. (2013). Classification of pig fat samples from different subcutaneous layers by means of fast and non-destructive analytical techniques. *Food Research International, 52*(1), 185–197.
Fulladosa, E., Santos-Garcés, E., Picouet, P., & Gou, P. (2010). Prediction of salt and water content in dry-cured hams by computed tomography. *Journal of Food Engineering, 96*(1), 80–85.
Garavaldi, A., Rossi, A., & Lo Fiego, D. P. (2008). Difetti di presentazione della coscia per prosciutto crudo: Valutazione sensoriale sul prodotto stagionato. In *II convegno nazionale della Società di Scienze sensoriali* (Vol. 2, pp. 303–308). Firenze University Press.
Gerrard, D. E., Gao, X., & Tan, J. (1996). Determining beef marbling and color score by image processing. *Journal of Food Science, 61*(1), 145–148.
Gomes, J. F. S., & Leta, F. R. (2012). Applications of computer vision techniques in the agriculture and food industry: A review. *European Food Research and Technology, 235*(6), 989–1000.
Guido, R. C. (2018). Paraconsistent feature engineering [lecture notes]. *IEEE Signal Processing Magazine, 36*(1), 154–158.
Haralick, R. M., Shanmugam, K., & Dinstein, I. H. (1973). Textural features for image classification. *IEEE Transactions on Systems, Man, and Cybernetics*, (6), 610–621.
Huang, H., Liu, L., Ngadi, M. O., & Gariepy, C. (2013). Prediction of pork marbling scores using pattern analysis techniques. *Food Control, 31*(1), 224–229.
Jackman, P., Sun, D. W., & Allen, P. (2009). Automatic segmentation of beef longissimus dorsi muscle and marbling by an adaptable algorithm. *Meat Science, 83*(2), 187–194.
Jackman, P., Sun, D. W., & Allen, P. (2011). Recent advances in the use of computer vision technology in the quality assessment of fresh meats. *Trends in Food Science & Technology, 22*(4), 185–197.
Joo, S. T., Kim, G. D., Hwang, Y. H., & Ryu, Y. C. (2013). Control of fresh meat quality through manipulation of muscle fiber characteristics. *Meat Science, 95*(4), 828–836.
Kapur, J., Sahoo, P. K., & Wong, A. K. (1985). A new method for gray-level picture thresholding using the entropy of the histogram. *Computer Vision, Graphics, and Image Processing, 29*(3), 273–285.
Kotsiantis, S. B., Zaharakis, I., & Pintelas, P. (2007). Supervised machine learning: A review of classification techniques. *Emerging artificial intelligence applications in computer engineering, 160*, 3–24.
Laddi, A., Sharma, S., Kumar, A., & Kapur, P. (2013). Classification of tea grains based upon image texture feature analysis under different illumination conditions. *Journal of Food Engineering, 115*(2), 226–231.
Li, D., Li, N., Wang, J., & Zhu, T. (2015). Pornographic images recognition based on spatial pyramid partition and multi-instance ensemble learning. *Knowledge-Based Systems, 84*, 214–223.
Lo Fiego, D. P., Comellini, M., Ielo, M. C., Ulrici, A., Volpelli, L. A., Tassone, F., et al. (2007). Preliminary investigation of the use of digital image analysis for raw ham evaluation. *Italian Journal of Animal Science, 6*(sup1), 693–695.
Lo Fiego, D. P., Nanni Costa, L., Tassone, F., & Russo, V. (2003). Effect of different stunning methods of pigs on subcutaneous veining defect and meat quality of raw ham. *Italian Journal of Animal Science, 2*(sup1), 370–372.
Lopes, J. F., Ludwig, L., Barbin, D. F., Grossmann, M. V. E., & Barbon, S. (2019). Computer vision classification of barley flour based on spatial pyramid partition ensemble. *Sensors, 19*(13), 2953.
Lu, J., Tan, J., Shatadal, P., & Gerrard, D. E. (2000). Evaluation of pork color by using computer vision. *Meat Science, 56*(1), 57–60.
Mancini, R., & Hunt, M. (2005). Current research in meat color. *Meat Science, 71*(1), 100–121.
Manzocco, L., Anese, M., Marzona, S., Innocente, N., Lagazio, C., & Nicoli, M. C. (2013). Monitoring dry-curing of S. Daniele ham by magnetic resonance imaging. *Food Chemistry, 141*(3), 2246–2252.
Mateo, A., Soto, F., Villarejo, J. A., Roca-Dorda, J., De la Gandara, F., & García, A. (2006). Quality analysis of tuna meat using an automated color inspection system. *Aquacultural Engineering, 35*(1), 1–13.
McCarthy, M. J. (2012). *Magnetic resonance imaging in foods*. Springer Science & Business Media.
Muñoz, I., Gou, P., & Fulladosa, E. (2019). Computer image analysis for intramuscular fat segmentation in dry-cured ham slices using convolutional neural networks. *Food Control, 106*, 106693. https://doi.org/10.1016/j.foodcont.2019.06.019.
Muñoz, I., Rubio-Celorio, M., Garcia-Gil, N., Guàrdia, M. D., & Fulladosa, E. (2015). Computer image analysis as a tool for classifying marbling: A case study in dry-cured ham. *Journal of Food Engineering, 166*, 148–155.
Nixon, M., & Aguado, A. (2012). *Feature extraction and image processing for computer vision*. Academic Press.
Ogawa, Y., Kondo, N., & Shibusawa, S. (2003, July). Inside quality evaluation of fruit by X-ray image. In *Proceedings 2003 IEEE/*

ASME international conference on advanced intelligent mechatronics (AIM 2003) (Vol. 2, pp. 1360–1365). IEEE.
Ojala, T., Pietikäinen, M., & Mäenpää, T. (2002). Multiresolution gray-scale and rotation invariant texture classification with local binary patterns. *IEEE Transactions on Pattern Analysis and Machine Intelligence*, (7), 971–987.
Orlandi, G., Calvini, R., Foca, G., & Ulrici, A. (2018a). Automated quantification of defective maize kernels by means of multivariate image analysis. *Food Control, 85*, 259–268.
Orlandi, G., Calvini, R., Pigani, L., Foca, G., Simone, G. V., Antonelli, A., et al. (2018b). Electronic eye for the prediction of parameters related to grape ripening. *Talanta, 186*, 381–388.
O'sullivan, M. G., Byrne, D. V., Martens, H., Gidskehaug, L. H., Andersen, H. J., & Martens, M. (2003). Evaluation of pork colour: Prediction of visual sensory quality of meat from instrumental and computer vision methods of colour analysis. *Meat Science, 65*(2), 909–918.
Parma Quality Institute. (2017). *Dossier 2016* (Vols. 5–38). Italy: Langhirano.
Pereira, L. F. S., Barbon, S., Jr., Valous, N. A., & Barbin, D. F. (2018). Predicting the ripening of papaya fruit with digital imaging and random forests. *Computers and Electronics in Agriculture, 145*, 76–82.
Pu, H., Sun, D. W., Ma, J., & Cheng, J. H. (2015). Classification of fresh and frozen-thawed pork muscles using visible and near infrared hyperspectral imaging and textural analysis. *Meat Science, 99*, 81–88.
Rodríguez-Pulido, F. J., Gordillo, B., González-Miret, M. L., & Heredia, F. J. (2013). Analysis of food appearance properties by computer vision applying ellipsoids to colour data. *Computers and Electronics in Agriculture, 99*, 108–115.
Rosenvold, K., & Andersen, H. J. (2003). Factors of significance for pork quality-a review. *Meat Science, 64*(3), 219–237.
Russo, V., Lo Fiego, D. P., Nanni Costa, L., & Tassone, F. (2003). Indagine sul difetto di venatura delle cosce di suino destinate alla produzione del prosciutto di parma. *Rivista di Suinicoltura, 44*, 77–82.
Russo, V., Lo Fiego, D. P., Nanni Costa, L., & Tassone, F. (2004, November). Study of some factors affecting the incidence of veining defect in thighs destined to dry-cured process of Parma ham. In *Proceedings of the 5th international symposium on the mediterranean pig, Tarbes, France*.
Salazar, F., Toledo, M. A., Oñate, E., & Morán, R. (2015). An empirical comparison of machine learning techniques for dam behaviour modelling. *Structural Safety, 56*, 9–17.
Sánchez, A. J., Albarracin, W., Grau, R., Ricolfe, C., & Barat, J. M. (2008). Control of ham salting by using image segmentation. *Food Control, 19*(2), 135–142.
Schoeman, L., Williams, P., du Plessis, A., & Manley, M. (2016). X-ray micro-computed tomography (μCT) for non-destructive characterisation of food microstructure. *Trends in Food Science & Technology, 47*, 10–24.
Scornet, E., Biau, G., & Vert, J. P. (2015). Consistency of random forests. *Annals of Statistics, 43*(4), 1716–1741.
Shen, H. K., Chen, P. H., & Chang, L. M. (2013). Automated steel bridge coating rust defect recognition method based on color and texture feature. *Automation in Construction, 31*, 338–356.
Singh, A., & Singh, M. L. (2016). Performance evaluation of various classifiers for color prediction of rice paddy plant leaf. *Journal of Electronic Imaging, 25*(6), 061403.
Sobel, I. (1978). Neighborhood coding of binary images for fast contour following and general binary array processing. *Computer Graphics and Image Processing, 8*(1), 127–135.
Sun, X., Young, J., Liu, J. H., Bachmeier, L., Somers, R. M., Chen, K. J., et al. (2016). Prediction of pork color attributes using computer vision system. *Meat Science, 113*, 62–64.
Ulrici, A., Foca, G., Ielo, M. C., Volpelli, L. A., & Fiego, D. P. L. (2012). Automated identification and visualization of food defects using rgb imaging: Application to the detection of red skin defect of raw hams. *Innovative Food Science & Emerging Technologies, 16*, 417–426.
Vapnik, V. N. (1995). *The nature of statistical learning theory*. Springer science & business media.
Wang, L. (2005). *Support vector machines: Theory and applications*. Springer Science & Business Media.
Wu, D., Shi, H., Wang, S., He, Y., Bao, Y., & Liu, K. (2012). Rapid prediction of moisture content of dehydrated prawns using online hyperspectral imaging system. *Analytica Chimica Acta, 726*, 57–66.
Zapotoczny, P., Szczypiński, P. M., & Daszkiewicz, T. (2016). Evaluation of the quality of cold meats by computer-assisted image analysis. *LWT-Food Science and Technology, 67*, 37–49.